Article

Frequency Shift Keying-Based Long-Range Underwater Communication for Consecutive Channel Estimation and Compensation Using Chirp Waveform Symbol Signals

Jongmin Ahn , Dong-Hun Lee, Sangkug Lee and Wanjin Kim *

Agency of Defense Development, Changwon-si 516852, Republic of Korea; anjong3@naver.com (J.A.)
* Correspondence: kimwj@add.re.kr; Tel.: +82-055-540-6336

Abstract: Currently, the demand for long-range underwater communication (UWC) is increasing. Conventional long-range UWC studies utilize vertical line array (VLA) and equalization techniques such as TRM and DFE to mitigate the long multi-path delay. However, recently developed underwater platforms such as unmanned underwater vehicles (UUVs) utilize a single hydrophone, and it is hard to apply the conventional long-range UWC system to these platforms. This paper proposes frequency shifting-based modulation to overcome the large multi-path delay without any optimization or training symbol. Unlike FSK, the proposed modulation method transmits the data using linear frequency modulation (LFM). The proposed demodulation method estimates the multi-path delay using data-modulated LFM and utilizes the estimated multi-path to compensate for the subsequent data signal. Therefore, the proposed method has better BER performance than FSK, and it is demonstrated through a simulation and ocean experiment with a single hydrophone.

Keywords: long-range underwater communication; underwater acoustic communication; channel equalization

1. Introduction

Recently, various underwater platforms (unmanned underwater vehicles (UUVs), underwater gliders, etc.) have been developed. Thanks to these developments, the demand for long-range underwater communication (UWC) to control underwater platforms is also increasing. Long distance (i.e., over tens of kilometers) means an increased propagation time. Thus, transmitted signals suffer from long multi-path delays. Various studies and experiments have been conducted to overcome these disadvantages of the long-range underwater environment. Stojanovic et al. received quadrature phase shift keying (QPSK) signals with a five-channel vertical line array (VLA) at a distance of 89 km [1]. Then, the received signals were equalized with a decision feedback equalizer (DFE) to decrease the bit error rate (BER). These experimentsl results showed that long-range UWC is possible. Simura et al. received BPSK signals with a 20 ch vertical line array (VLA) at a 1000 km distance [2]. Kang et al. utilized orthogonal frequency division multiplexing (OFDM) to overcome the long multi-path delay [3]. However, experimental results showed that OFDM, a multi-carrier modulation technique, struggles to obtain a received signal with high SNR due to the peak-to-average power ratio (PAPR). In particular, when received by one hydrophone, BER became 0.3 and communication was impossible. Note that the absence of error was not possible with the conventional minimum mean square error (MMSE) channel estimation methods, even after combining eight OFDM blocks [3]. These results show that multi-carrier communication systems (e.g., OFDM) are not suitable for long-range UWC. Various modulation techniques, such as generalized sinusoidal frequency modulation (GSFM) and chirp shift keying (CSK), have been applied for long-range UWC [4,5]. However, all of the studies conducted received signals with VLA and equalization techniques such as time reversal mirror (TRM) and DFE applied to UWC. As a

result of surveying the long-range UWC research, VLA and equalization techniques such as TRM and DFE are essential to mitigate long multi-path delays [6,7]. However, it is hard to apply these techniques to long-range underwater platforms such as UUVs.

There are two reasons. Firstly, the equalization techniques, such as DFE, need to optimize some parameters (i.e., the number of training symbols, a pilot symbol, and feedback (FB)/forward (FF) tabs). The results of long-range UWC experiments showed that the number of training symbols and FF/FB tabs varies depending on the environment and channel [8–11]. The long-range UWC has a long propagation delay of several minutes, and it is very hard to exchange information between the transmitter and receiver before the channel characteristics change. Thus, optimizing these parameters is very hard. Secondly, underwater platforms such as unmanned underwater vehicles (UUVs) struggle to use VLA. A VLA usually has tens of hydrophones. Thus, it has a length of several hundred meters and weighs several hundred kilograms. However, currently, developed underwater platforms such as UUVs and remotely operated vehicles (ROV) cannot afford the VLA due to its large size and heavy weight. For these reasons, the conventional long-range UWC methods are hard to apply in underwater platforms such as UUVs [12–17].

Pelekanakis et al. analyzed BER when modulation signals of FH-BFSK, BPSK, QPSK, and 8PSK were received through a single hydrophone at a distance of 33 km [10]. As a result, FH-BFSK showed the lowest BER, and it also showed error-free results with maximum ratio combining (MRC) to moderate the distortion of multi-path delay [10]. These results show that, if FSK overcomes multi-path delay, it can be a reliable scheme for a long-range underwater communication system for UUVs (i.e., utilizing one hydrophone). The experiments of long-range UWC and measured multi-path delay are summarized in Table 1.

Table 1. Summarization of the acoustic channel of long-range ocean experiments.

Distance (km)	# Path	Max. Delay (ms)	Exp. Name	Year	Ref.
89	3~5	40	N/A	1991	[1]
203		50			
50	2~4	200	LORACOM	1996	[18]
40	3~4	2000	N/A	2008	[19]
100		1000			
300	5	1000	N/A	2010	[20]
550	2	30	LRAC'10	2010	[3,8]
180	4	300	KY10-13	2010	[21]
500	6~9	1500			
500	1~2	600	KY11-11	2011	[2]
700					
500	15~17	2000	N/A	2011	[22]
50	2~4	60	N/A	2015	[23]
60	4	190	BLAC'18	2018	[4,11]
33	7~8	200	N/A	2019	[10]
20	6	50	BLAC'20	2020	[5]
160	2	100	ACUA'21	2021	[24]

In Table 1, the maximum multi-path delay and the number of the multi-path are 2 s and 17, respectively. Therefore, mitigating long multi-path delays is important to achieve low BER in long-range UWC systems.

In this paper, a novel modulation scheme is proposed, where bits are assigned to frequencies in the same manner as FSK. However, unlike FSK, the proposed method has a linear frequency modulation (LFM) shape. Since the proposed modulated data are transmitted using LFM, which is suitable for estimating the multi-path delay, the proposed method can estimate the multi-path delay using the data signal after demodulating the data. This estimated multi-path delay is utilized to decrease the channel effect of the subsequent

data signal without a training symbol or FF/FB optimization. Thus, the proposed method is suitable for long-range underwater communication systems utilizing single hydrophones.

This paper consists of six sections. Section 2 describes the difference between the conventional long-range UWC system and the long-range UWC system for an underwater platform such as UUVs and ROVs. In Section 3, the proposed method is described. In Section 4, computer simulations of long-range UWC environments are shown. The results of ocean experiments are described in Section 5. Section 6 concludes the paper.

2. System Model

The difference in long-range UWC systems between the conventional and the underwater platform is briefly described so that reader can easily understand. Underwater, acoustic sound waves do not propagate in a straight line but in a curve [25]. The sound wave changes direction up and down depending on the temperature and pressure of the ocean. Because of these physical phenomena, sound waves are trapped in layers with minimal sound velocity, which is called a sound fixing and ranging (SOFAR) channel [26]. The sound generated in the SOFAR channel travels a long distance. Therefore, a long-range UWC system places a transmitter and receiver in the SOFAR channel [18].

The conventional long-range UWC system is a multiple-output system that receives the communication signal with the VLA composed of several hydrophones. On the other hand, underwater platforms such as UUVs and ROVs struggle to obtain diversity gain with a VLA. Thus, the long-range UWC system for this platform is modeled as a single-output system. The conventional long-range UWC system and long-range UWC system for underwater platforms are shown in Figure 1.
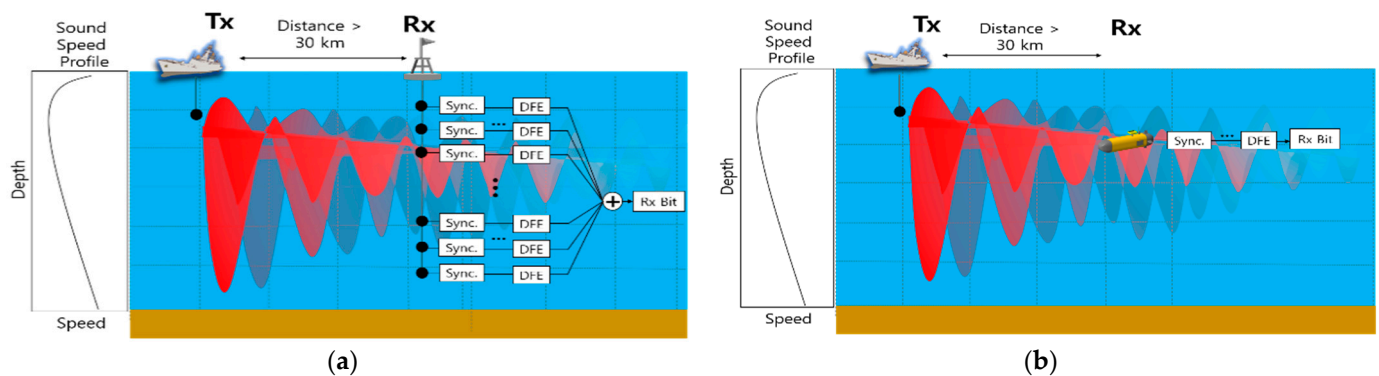

Figure 1. Long-range underwater communication system: (**a**) conventional (Multiple Output); (**b**) UUV (Single Output).

In Figure 1a, the conventional long-range UWC system is modeled as a multiple-output system. The conventional long-range UWC system equalizes each of the signals received by multiple hydrophones with DFE and the equalized signals are added to obtain a diversity gain. However, as shown in Figure 1b, since the underwater platform has a single output, it struggles to utilize the conventional long-range UWC technique. A horizontal line array (HLA) is also utilized for long-range UWC [27–29]. However, the required distance between hydrophones in the HLA is approximately 100 m. Thus, the length of the HLA makes it impractical for applications with existing UUVs [12–17].

Please note that the proposed method achieves a low bit error rate (BER), even if only one hydrophone is used, and it can be simultaneously utilized with the conventional long-range UWC system utilizing multiple hydrophones. By applying the proposed method with the conventional long-range UWC system utilizing multiple hydrophones, the BER performance can be further improved. In the next section, the proposed method is described.

3. Proposed Method

3.1. Modulation

Conventional underwater acoustic systems generally utilize LFM to measure the multi-path delay because the auto-correlation function of LFM is the Kronecker-delta function [30,31]. The proposed method generates a data signal using an LFM to utilize its auto-correlation characteristic, and the data signal can be utilized to estimate the multi-path delay using a state-of-the-art multi-path estimating scheme. LFM is expressed as

$$c(t) = \sqrt{E} \times cos\left(2\pi\left(\frac{f_{st} - f_{end}}{2T_c}t^2 + f_{st}t\right)\right). \tag{1}$$

In Equation (1), T_c, f_{st}, and f_{end} are the time length, start frequency, and end frequency of LFM, respectively. E is the energy of LFM. The proposed method modulates two symbols to the start and end frequency. When the modulation order of the proposed method is M, the M-length bit sequence (b) is modulated with a symbol (s). b can be converted into one of the decimal numbers from zero to $(2^M - 1)$ according to the gray mapping rule. Let $B_{TX} = \{b_1, \cdots, b_k, \cdots, b_K\}$ be the transmitting K binary sequences. When $g(\cdot)$ is the function of the gray mapping rule, s is obtained as $g(b_k)$. The set of the symbol is expressed as

$$S = \left\{s_k \middle| s_k = g(b_k), b_k = m_2, 0 \leq m_2 \leq 2^{M-1}\right\}. \tag{2}$$

In Equation (2), m_2 is a binary number. Each b_k is modulated to symbol s_k. The proposed method transmits two symbols using one LFM. Thus, when the K is an odd number, a dummy symbol is inserted at the beginning of the symbol sequence. Then, these symbols are grouped into pairs. Assume that s_k and s_{k+1} are grouped. These symbols represent the index of LFM frequency (i.e., $f_{min} \cdots f_{max}$). When the minimum frequency of LFM is f_{min}, the set of frequency values for the proposed method can be expressed as Equation (3) using S,

$$F = \{f | f = f_{min} + (s-1) \times \Delta f, s \in S\}. \tag{3}$$

In Equation (3), Δf is the minimum frequency interval that maintains orthogonality between different LFMs. Δf is greater than or equal to $2/T_c$. The s_k-th element of the set F is denoted $F(s_k)$. By substituting $F(s_k)$ and $F(s_{k+1})$ into f_{st} and f_{end}, the data LFM modulated with these two symbols is generated. This data LFM is expressed as Equation (4),

$$x_l(t) = \sqrt{E} \times cos\left(2\pi\left(\frac{F(s_k) - F(s_{k+1})}{2T_c}t^2 + F(s_k)t\right)\right), l = 1 \cdots L. \tag{4}$$

In Equation (4), L is the index of LFM and is calculated as $\lceil K/2 \rceil$. Similar to FSK, the proposed method assigns bits to the frequency. However, the shape of the data signal is LFM, unlike that of FSK which is the CW. Note that LFM can be utilized to estimate the multi-path delay. This difference allows the proposed method to estimate the multi-path delay using the data signal. Since the proposed demodulation method consecutively estimates multi-path delay and compensates for the data signal, the first LFM ($x_1(t)$) is a dummy signal. Figure 2 shows the spectrogram of the proposed modulated signal. The structure of the proposed modulation method is described in Figure 3.

The proposed modulation transmits two symbols using one LFM, and the symbol time duration is $T_c/2$. Let B be available bandwidth. The maximum modulation order (M) is calculated as $\log_2 \lceil B/\Delta f \rceil$. As mentioned above, Δf is $2/T_c$ and the maximum modulation order can be rewritten as $\log_2 \lceil BT_c/2 \rceil$. It means $M(= \log_2 \lceil BT_c/2 \rceil)$ bits are transmitted for $T_c/2$. The data rate (d) of the proposed method is expressed as

$$d = 2\left(log_2 \left\lceil \frac{BT_c}{2} \right\rceil\right)/T_c. \tag{5}$$

The data rate of the proposed method is the same as that of the FSK, which has $T_c/2$ symbol length and M modulation order. Thus, there is no loss of data rate. The proposed demodulation method estimates the multi-path delay using the received data signal and compensates for the subsequent data signal. Thus, the BER of the proposed method will be reduced in the long-range UWC channel. The following section describes the proposed demodulation method.
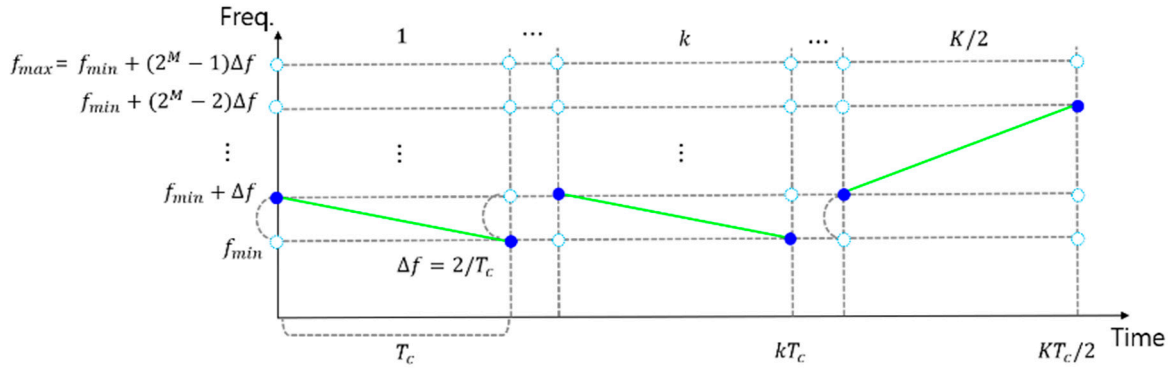

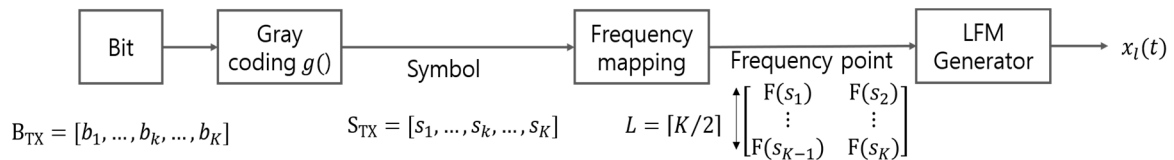**Figure 2.** Spectrogram of the proposed modulated signal.

Figure 3. Block diagram of the proposed modulation method.

3.2. Demodulation

The LFM ($x_l(t)$) passes through the long-range UWC channel and is received at the receiver. The received signal $y_l(t)$ is expressed as

$$y_l(t) = x_l(t) \bigotimes h_l(t) + n(t). \tag{6}$$

In Equation (6), $\otimes$ denotes the convolution operator. $h_l(t)$ is the UWC channel of the l-th LFM. $n(t)$ denotes the time series of additive white Gaussian noise (AWGN). The proposed receiver demodulates two symbols from one LFM using the maximum likelihood (ML) detector and finds the maximum joint probability to demodulate the two symbols. When the transmitted symbol pair is s_k and s_{k+1}, detecting these two symbols with the maximum joint probability is expressed as

$$\hat{s}_k, \hat{s}_{k+1} = \underset{s_m, s_n}{argmax} P(s_k, s_{k+1} | s_m, s_n). \tag{7}$$

In Equation (7), s_m and s_n denote an arbitrary symbol that belongs to the set S. $\hat{s}_k$ and $\hat{s}_{k+1}$ are the finally decided symbols at the receiver. To find the pair of symbols that satisfies Equation (7), the proposed demodulation method calculates a correlation between $x_l(t)$ and all LFMs that can be generated by arbitrary pairs of symbols (s_m and s_n). Then, s_m and s_n of LFM with the maximum correlation become $\hat{s}_k$ and $\hat{s}_{k+1}$. For simplicity, we define $x(s_m, s_n)$ as LFM modulated with (s_m and s_n). The transmitted LFM $x_l(t)$ can be rewritten as $x_l(s_k, s_{k+1})$. The correlation between $x_l(s_k, s_{k+1})$ and $x(s_m, s_n)$ is calculated as below according to modulated symbols:

$$x(s_k, s_{k+1}) \star x(s_m, s_n) = \begin{cases} H_0(s_k = s_m \wedge s_{k+1} = s_n) : R(0) \approx E \\ H_1(s_k \neq s_m \vee s_{k+1} \neq s_n) : R(0) \approx 0 \end{cases}. \tag{8}$$

In Equation (8), $R(0)$ is the correlation value and E is the power of LFM. ($\star$) denotes the correlation operator. H_0 is a hypothesis for the situation where both symbols in LFM are correctly selected, H_1 is a hypothesis for the situation where at least one of the symbols in the LFM is chosen incorrectly. When $R(0)$ becomes the maximum value, two symbol pairs (s_k, s_{k+1} and s_m, s_n) are the same in the AWGN environment. The principle of the received symbol decision is the same as the non-coherent FSK. Thus, the BER of the proposed method approximates the BER of the non-coherent FSK (Appendix A). However, the transmitted signal ($x_l(t)$) is distorted by the long-range UWC channel ($h_l(t)$). In order to find the symbol pair that satisfies Equation (7), the receiver needs to reduce the effect of the long-range UWC channel ($h_l(t)$). The proposed demodulation method estimates $h_{l-1}(t)$ using the $(l-1)$-th received signal. When s_k and s_{k+1} are the same, the symbol signal becomes a single tone and the multi-path delay estimation also becomes inaccurate. However, this happens with a probability of $1/M$. Additionally, as shown in Appendix A, the proposed method shows the same BER performance of FSK in the AWGN environment. This result indicates that the absence of multi-path delay estimation does not decrease BER compared to the conventional FSK when a single-tone symbol signal is generated. It can be assumed that $h_{l-1}(t)$ is equal to $h_l(t)$ because T_c is usually less than tens of milliseconds. Therefore, the estimated $h_{l-1}(t)$ can be used to mitigate the distortion of $y_l(t)$ caused by multi-path. The result of the channel-equalized result ($R_c(0)$) is expressed as

$$
\begin{aligned}
R_c(0) &= y_l(t) \star (x(s_m, s_n) \otimes h_{l-1}(t)) \\
&= (h_l(t) \otimes h_{l-1}(-t)) \star (x(s_k, s_{k+1}) \star x(s_m, s_n)) \\
&= \delta(t) \star R(0)
\end{aligned}
\tag{9}
$$

In Equation (9), $h_l(t) \otimes h_{l-1}(-t)$ shows a similar effect to performing channel equalization, and it becomes approximately the Kronecker-delta function ($\delta(t)$) because we assumed ($h_l(t) \approx h_{l-1}(-t)$) [31–33]. Therefore, when two symbol pairs (s_k, s_{k+1} and s_m, s_n) are the same, R_c becomes the maximum value and satisfies Equation (7) in the long-range UWC channel. The received symbol pair is detected as Equation (10),

$$
\hat{s}_k, \hat{s}_{k+1} = \underset{s_m, s_n}{argmax} R_c(0)
\tag{10}
$$

The block diagram of the proposed demodulation method is depicted in Figure 4. In the next section, the computer simulations and ocean experimental results are shown for BER performance comparisons of the proposed method with the conventional FSK.
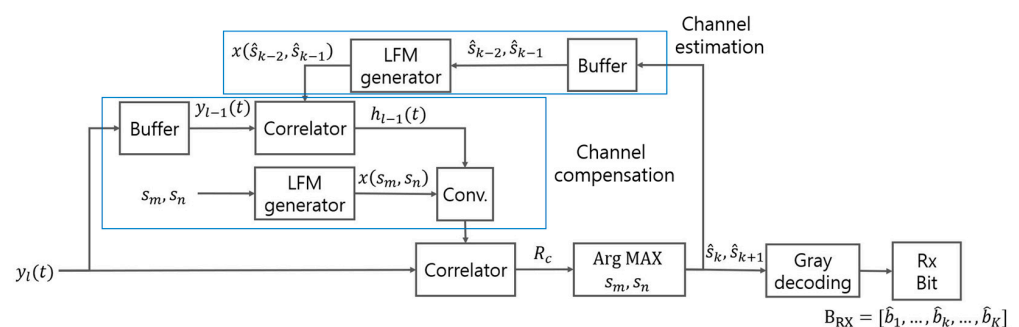

Figure 4. Block diagram of the proposed demodulation method.

4. Simulation

The BER performance of the proposed method was compared with that of the non-coherent FSK in long-range underwater environments. In the case of the long-range UWC, the sound wave propagation varies greatly depending on the experimental location and environmental factors. It is challenging to consider all environmental factors (e.g., temperature, salinity, current, sea bed, etc.) that affect the UWC channel. Therefore, we referred to the measured multi-path from the long-range underwater acoustic communication experi-

ments to generate the UWC channel for the simulation. Based on Table 1, four channels were generated by BELLHOP according to maximum delay, and these four channels were utilized for simulation. The maximum Doppler spread of the simulation channel was 2 Hz. The modulation parameters for the simulation are represented in Table 2. The start frequency (f_{min}) is 2600 Hz.

Table 2. Modulation parameters for simulation of long-range UWC.

Modulation order (M)	4	3
Bandwidth (B, Hz)	750	350
Proposed signal length (T_c, ms)	40	
FSK signal length (T_c, ms)	20	

In Figure 5, the purple line is the BER of the proposed method and the black line is the BER of FSK. The solid line represents the BER when M is four and the dashed line shows the BER when M is three. The top of Figure 5 presents various long-range UWC channels. In Figure 5a, the BER of the proposed method is 1×10^{-3} at 7 dB SNR when M is four. However, FSK is 8×10^{-3} at the same SNR. In Figure 5, it can be seen that the BER of the proposed method is generally lower than that of the FSK. On the other hand, the superiority of the BER performance is reversed at low SNR. The BER performance of the proposed method is analyzed in detail depending on SNR.
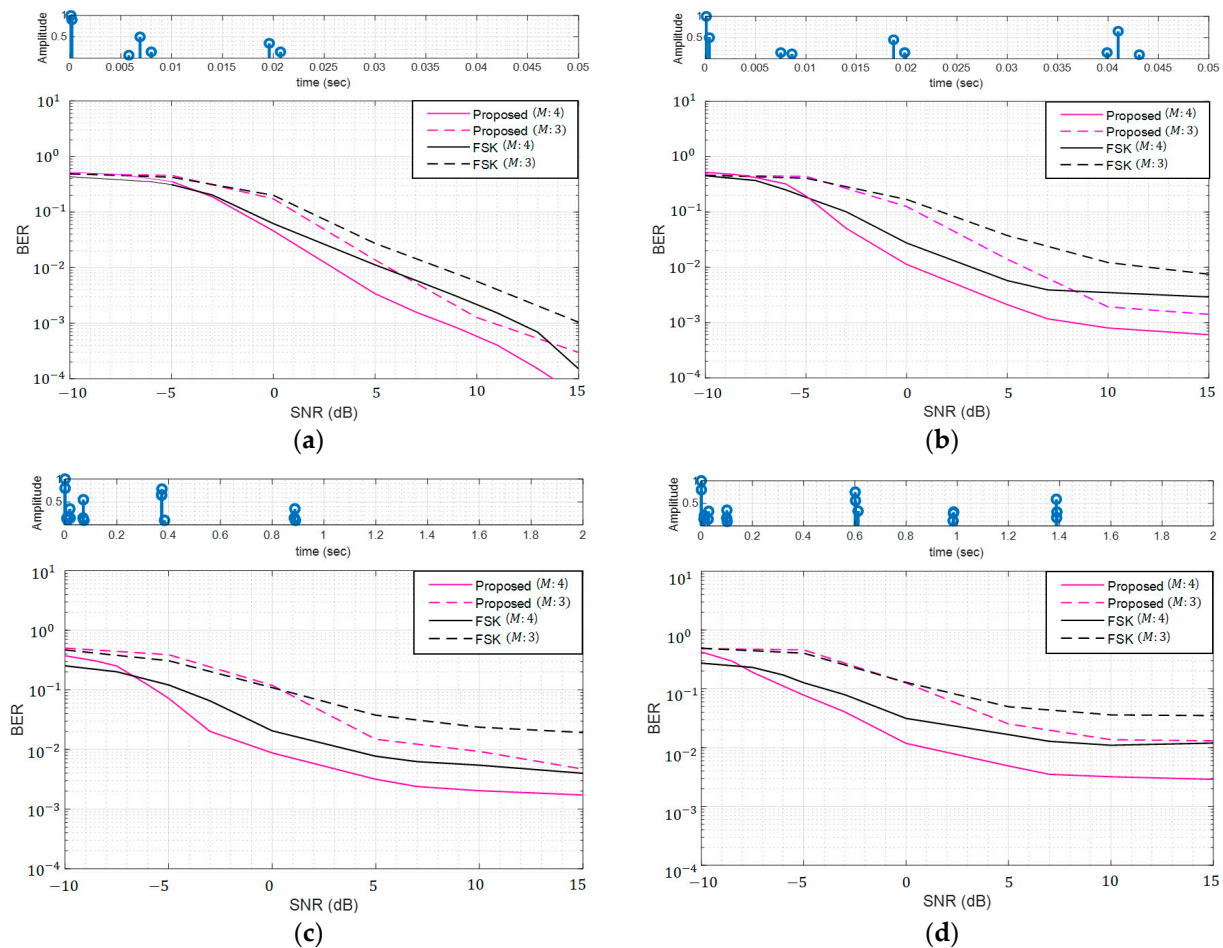

Figure 5. Simulation BER results according to the modulation order with varying maximum channel delay: (**a**) 20 ms; (**b**) 40 ms; (**c**) 0.9 s; (**d**) 1.4 s.

In low-SNR environments, the proposed method shows higher BER compared to conventional FSK due to error propagation caused by inaccurate multi-path estimation

using previous symbol signals. However, please note that, when the BER of the proposed method is greater than that of conventional FSK., both methods have BER values above 0.1, which are impractical for communication. As the *M* increases, the probability of generating a symbol signal with a higher chirp-rate also increases and LFM with a high chirp-rate has higher multi-path estimation accuracy than LFM with a low chirp-rate. This property becomes more prominent in the low-SNR environment. Thus, in low-SNR environments, the probability of accurate multi-path estimation is higher when *M* is four compared to when *M* is three. This phenomenon is observed in Figure 5. When *M* is four (solid line), the improvement in BER performance of the proposed method compared to that of FSK is greater than when *M* is three (dashed line), in the SNR range of −3 dB to 5 dB. When the SNR is above 5 dB, the BER performance of the proposed method improves regardless of *M*.

In a high-SNR environment, symbol signals with a low chirp-rate can also accurately estimate and compensate for the multi-path. This result can be explained by principles of channel estimation and equalization using pilots in conventional communication techniques. When the SNR is low, the improvement in BER is more affected by the accuracy of the estimated channel using the pilot rather than the performance of the equalizer itself. In the high-SNR range where the accuracy of multi-path estimation is already high, the performance of the equalizer becomes the dominant factor for BER performance. Therefore, in the high-SNR range, the improvement in BER of the proposed method compared to FSK does not significantly depend on *M* (i.e., chirp-rate of symbol signal).

When the channel delay is longer than the symbol length, the channel equalization will not be accurate. This is because channel estimation beyond the symbol time length is not possible. This problem also occurs in existing equalizers, and it is very important to set the appropriate pilot interval and length according to the channel length in the existing channel equalization technique. In Figure 5b–d, when the SNR increases, the error does not converge to 0 and an error floor converges to a specific value. This is because channels longer than the symbol time length are not estimated.

The proposed method estimates and compensates for the multi-path delay depending on the symbol length. Thus, using a symbol signal longer than the minimum required length ($2/\Delta f$) is similar to increasing the number of taps in the equalizer. Simulations were conducted using the signal parameters from Table 3 and the same UWC channel of the previous simulations was utilized.

Table 3. Modulation parameters for simulation of long-range UWC.

Modulation order (*M*)	4	
Bandwidth (*B*, Hz)	750	
Proposed signal length (T_c, ms)	40	80
FSK signal length (T_c, ms)	20	40

In Figure 6, the solid lines are the BER of the minimum length symbol signal (40 ms) and the dashed lines are the BER obtained using twice the minimum length symbol signal (80 ms). The blue lines represent the BER of the FSK and the red lines are the proposed method. For FSK, doubling the time length of the symbol signal is equivalent to sending the signal twice consecutively, resulting in a 3 dB SNR gain. Therefore, in Figure 6, the blue dashed lines show a 3 dB SNR gain compared to the blue solid lines. On the other hand, in Figure 6a, the proposed method shows a 6 dB SNR gain. This is because a longer time length of the symbol signal allows for estimation and compensation of a longer time delay of multi-path. It leads to similar results when equalizer performance is improved. Thus, the proposed method can have more than a 3 dB SNR gain.
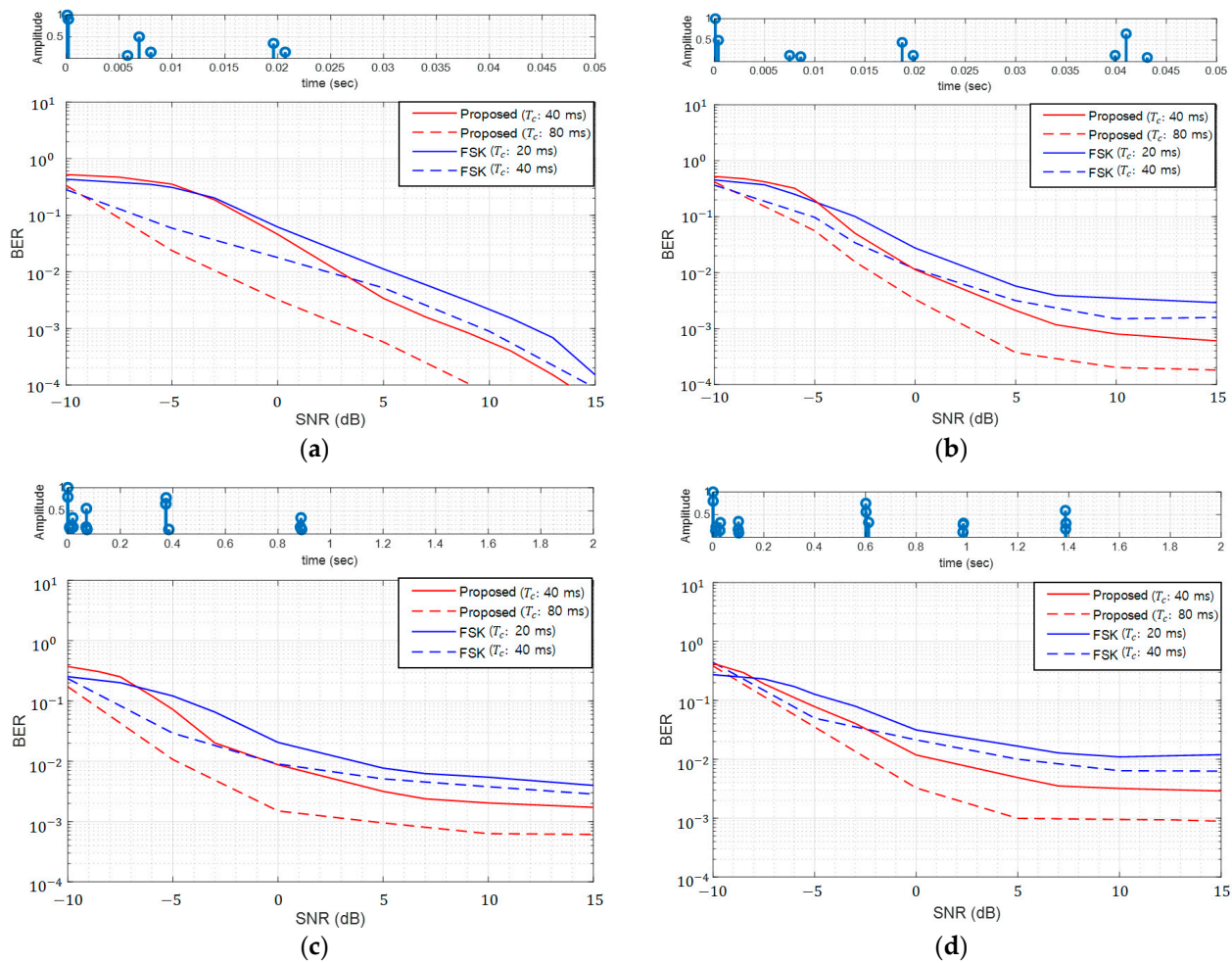
Figure 6. BER results according to the symbol time length with various maximum channel delays: (**a**) 20 ms; (**b**) 40 ms; (**c**) 0.9 s; (**d**) 1.4 s.

However, even if the symbol length is longer than the channel, the performance does not necessarily improve. Even if the symbol length is longer than the multi-path delay, channel estimation and compensation must be performed within the coherent time. The Doppler spread of the simulation channel is 2 Hz, and the coherent time is about 80 msec, which is equal to the symbol length. Therefore, the channel estimated by the preceding symbol is not the same as the channel experienced by the following symbol. For this reason, in Figure 6b, even when the symbol length is longer than the channel delay, the error floor occurs around 1×10^{-4}. In the next section, the BERs of the practical ocean experiments are demonstrated.

5. Ocean Experiment

Practical ocean experiments of the proposed method and FSK were executed in the East Sea on 18 May 2022. The transmitter (TX) was more than 60 km away from the receiver (RX). The average depth of the ocean was about 1100 m. The ocean bottom at TX and RX were about 850 m and 1200 m, respectively. The TX was located at a depth of 295 m, and the frequency band of the TX was 2.6 kHz to 4.6 kHz. The RX utilized a four-channel sensor, and each sensor was located at 180 m, 205 m, 230 m, and 255 m, respectively. Figure 7 shows the configuration and location of the experiments.
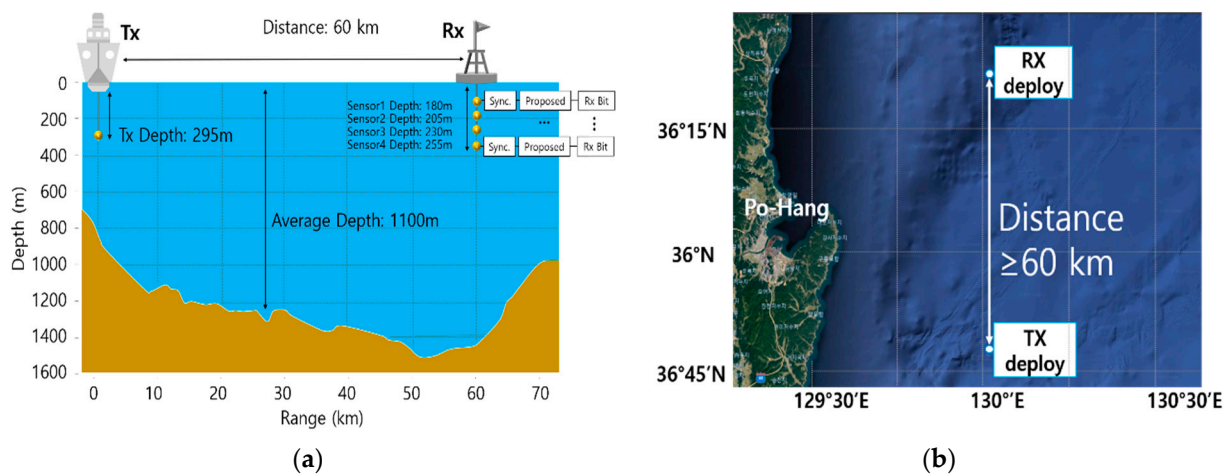
Figure 7. Ocean experiment: (**a**) configuration; (**b**) location.

The parameters of the proposed and the conventional methods are represented in Table 4.

Table 4. Modulation parameters of ocean experiments.

| Modulation Order (*M*) | Proposed | | FSK | |
	Bandwidth (*B*,Hz)	Proposed Signal Length (*T_c*,ms)	Bandwidth (*B*,Hz)	Proposed Signal Length (*T_c*,ms)
3	400 (2800–3200)	40	400 (2800–3200)	40
4	800 (2800–3600)	40	800 (2800–3600)	40
4	640 (2800–3440)	50	640 (2800–3440)	50
5	1280 (2800–4080)	50	1280 (2800–4080)	50

The communication signals were generated by modulating 3200 bits with each parameter in Table 4. These bits were turbo-coded with 1/3 code length and 4 constraint length. The experiment signals were transmitted as shown in Figure 8.
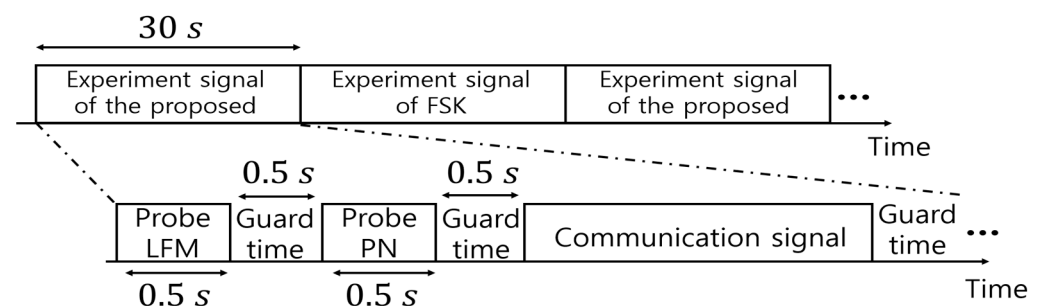

Figure 8. Experiment signal configuration.

As shown in Figure 8, LFM and probe signals with 0.5 s time length were transmitted before the communication signals of each parameter. The time length of the experiment signal was 30 s. The experiment signals of the proposed method and FSK were alternatively transmitted. Therefore, signals of both methods went through the same channel. Each experiment signal was transmitted seven times and the experiment signal contained 3200 bits. The transmitted signals were received with four sensors. Thus, a total of 89,600 bits were received for each parameter in Table 4. The underwater channel and received SNR were estimated using probe signals repeated every 30 s. Figure 9 shows the estimated channel over 20 min.
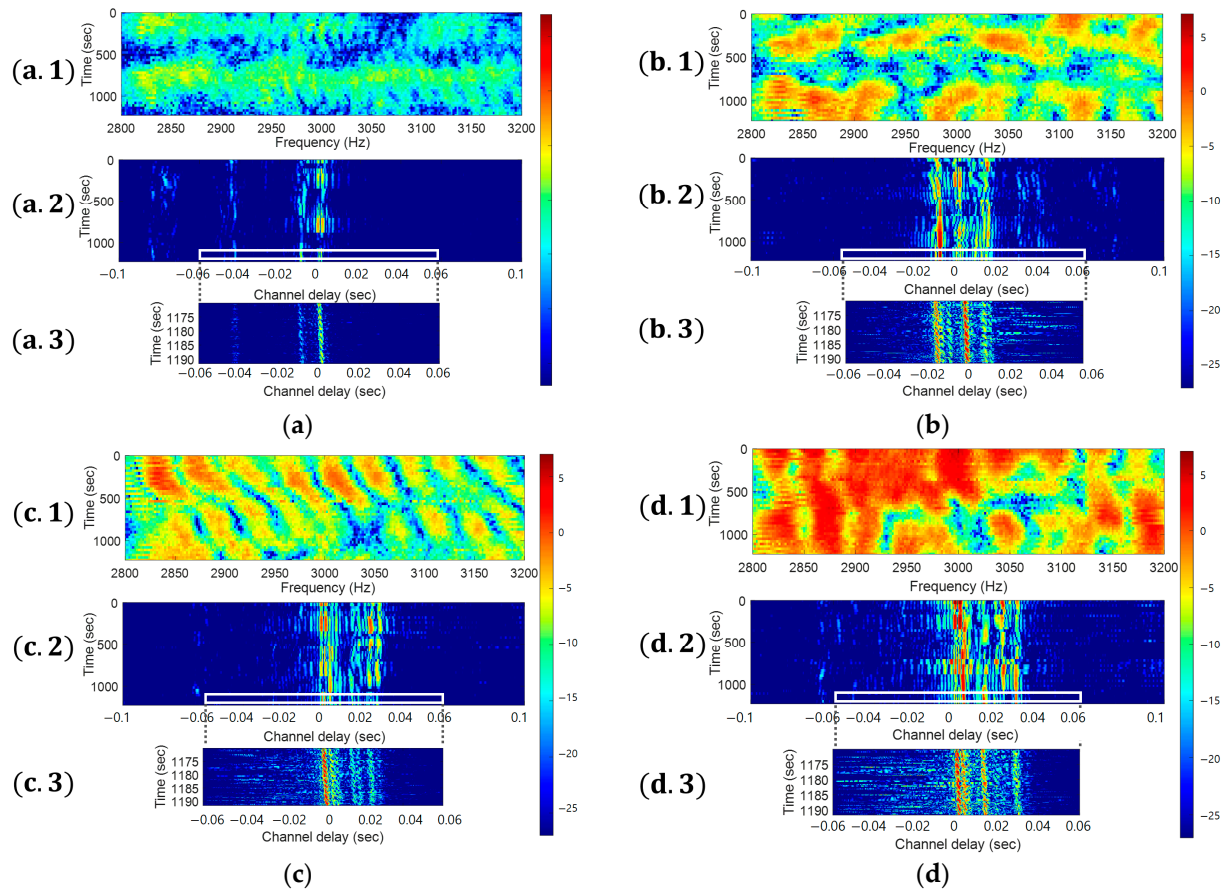
Figure 9. Estimated channel of ocean experiments: (**a.1**–**a.3**) Sensor 1; (**b.1**–**b.3**) Sensor 2; (**c.1**–**c.3**) Sensor 3; (**d.1**–**d.3**) Sensor 4.

In Figure 9(a.1–d.1), the power spectrum density (PSD) is represented and Figure 9(a.2–d.2) represent the multi-path delay profile. Figure 9(a.1–d.1,a.2–d.2) show results measured using probe signals shown in Figure 8. All the Y-axes in Figure 9 are the time of the ocean experiment. The color scale is in the dB scale.

In Figure 9(a.1), PSD is from −10 dB to −5 dB, and frequency selective fading occurred at intervals of approximately 15 Hz. Sensor 1 was at the highest depth and was outside of the SOFAR channel. Thus, the channel gain of Sensor 1 is measured from approximately −10 dB to −5 dB. In Figure 9(a.2), the maximum multi-path delay of Sensor 1 is almost 80 ms and it indicates the frequent frequency selective fading.

On the other hand, in Figure 9(d.1), the PSD gain ranges from 5 dB to 10 dB, with fading occurring at intervals of 50 Hz. Sensor 4 was located in the SOFAR channel. Thus, the received signal from Sensor 4 shows the highest channel gain, ranging from 5 dB to 7.5 dB. In Figure 9(b.2–d.2), the maximum multi-path delays of Sensors 2, 3, and 4 are below 40 ms. Therefore, based on the analysis of the UWC channel, when the maximum multi-path delay is below 40 ms, the estimated received channel gain is approximately from 3 dB to 7.5 dB. In contrast, when the maximum multi-path exceeds 40 ms, the received channel gain is estimated from −10 dB to −5 dB. The average Doppler spread is estimated at 1.5 Hz and the coherent time is approximately 0.1 s.

In Figure 9(a.3–d.3), the estimated multi-path delays using symbol signals from 1165 s to 1190 s are represented. These estimated multi-path delays are well matched with the multi-path estimation results in Figure 9(a.2–d.2) which were measured by probe signals. This fact means that the proposed method can estimate multi-path delay using symbol signals. To demonstrate that this estimated multi-path from symbol signals can be used for compensating consecutive symbol signals, the BERs of the proposed method and FSK

are represented in Table 5 according to the multi-path delay. Average SNRs are calculated using estimated channel gain and represented in Table 5 [34].

Table 5. Modulation parameters of ocean experiments.

Estimated SNR (dB)	Maximum Delay (ms)	Modulation Order (*M*)	Un-Coded BER		Turbo-Coded BER	
			Proposed	FSK	Proposed	FSK
8.87	<10	*M*: 3 T_c: 40 ms	N/A	N/A	N/A	N/A
		M: 4 T_c: 40 ms	0	0.008	0	0
		M: 4 T_c: 50 ms	0	0.009	0	0
		M: 5 T_c: 50 ms	0.006	0.080	0	0.008
4.51	10~20	*M*: 3 T_c: 40 ms	0	0.007	0	0
		M: 4 T_c: 40 ms	0	0.035	0	0
		M: 4 T_c: 50 ms	0.016	0.075	0	0.044
		M: 5 T_c: 50 ms	0.002	0.028	0	0
2.97	20~30	*M*: 3 T_c: 40 ms	0.023	0.031	0	0
		M: 4 T_c: 40 ms	0.019	0.024	0	0
		M: 4 T_c: 50 ms	0.045	0.080	0	0.047
		M: 5 T_c: 50 ms	0.066	0.084	0	0.069
2.45	30~40	*M*: 3 T_c: 40 ms	0.030	0.045	0	0
		M: 4 T_c: 40 ms	0.064	0.085	0.030	0.028
		M: 4 T_c: 50 ms	0.072	0.095	0.022	0.057
		M: 5 T_c: 50 ms	0.085	0.109	0.030	0.067
−9.12	>40	*M*: 3 T_c: 40 ms	0.224	0.211	0.205	0.167
		M: 4 T_c: 40 ms	0.292	0.258	0.287	0.238
		M: 4 T_c: 50 ms	0.288	0.249	0.303	0.243
		M: 5 T_c: 50 ms	0.349	0.302	0.367	0.317

In Table 5, when multi-path delay is from 0 to 20 ms, the BER of the conventional FSK ranges from 0.008 to 0.075, while the proposed method achieves a BER from 0 to 0.016. The proposed method shows better BER performance. When multi-path delay is from 0 to 20 ms, the SNR of the received ocean experiment signals is from 5 dB to 10 dB. In Figure 5a, the BER values of the proposed method and FSK are similar to that of the ocean experiments. However, in Table 5, when the maximum multi-path delay exceeds 40 ms, the proposed method shows higher BER than that of FSK. This is because the SNR of the received signal was from −10 dB to −5 dB. These BER results are well matched with the simulation results in Figure 5c,d, where SNR ranges from −10 dB to −5 dB. The coherent time estimated above is about 0.1 s. Therefore, when the channel delay is 10 ms to 20 ms, there are cases where the BER does not become 0 even if the symbol length is 50 ms. This is the same result as in Figure 6b. As a result, the ocean experiment results in Table 5 show a similar trend to simulation results in Figure 5. Note that the turbo-coded BER of the proposed method is error free when the maximum multi-path delay is less than 30 ms (i.e., high SNR). Therefore, the BER results of the ocean experiment show that the proposed method has lower BER than FSK in the long-range UWC channel.

6. Conclusions

This paper proposes a novel modulation method to overcome the large multi-path delay in the long-range UWC channel. The proposed method generates an LFM to transmit the data, unlike the FSK, which utilizes a CW pulse. This difference makes the proposed receiver estimate the multi-path using the received data signal. The receiver decreases the channel distortion of the subsequent data signal, and the proposed method can achieve lower BER than the FSK. A simulation and ocean experiment were conducted to demonstrate that the BER performance of the proposed method is superior to FSK. As a result of the ocean experiment, the turbo-coded BER of the proposed method was zero when

the maximum multi-path delay was lower than 30 ms. Also, it was shown that the error correction effect is better when used together with turbo coding.

The main contributions of the paper are summarized:

1. The novel frequency shift-based modulation/demodulation scheme for long-range UWC with a single receiving hydrophone has been proposed.

   - The proposed modulation method transmits the data using LFM suitable for the multi-path delay estimation.
   - The proposed demodulation method estimates the multi-path using the previous data signal without a training symbol or FF/FB tap optimization.
   - The proposed demodulation method consecutively compensates for received signals using the estimated multi-path.

2. We conducted computer simulations and practical ocean experiments to demonstrate that the proposed method has a lower BER than the conventional FSK in the long-range UWC environment.

The paper proposed a method of improving the BER by using one hydrophone as an underwater platform. If multiple hydrophones can be used in an underwater platform in the future, it is thought that a greater synergy can be created.

Author Contributions: Conceptualization, J.A. and W.K.; methodology, J.A. and W.K.; software, J.A.; validation, J.A. and W.K.; formal analysis, J.A.; investigation, W.K., D.-H.L. and S.L.; resources, D.-H.L. and S.L.; data curation, J.A., W.K. and S.L.; writing—original draft preparation, J.A.; writing— review and editing, J.A. and W.K.; visualization, J.A. and W.K.; supervision, J.A. and W.K.; project administration, W.K., D.-H.L. and S.L.; funding acquisition, W.K., D.-H.L. and S.L. All authors have read and agreed to the published version of the manuscript.

Abbreviations

$K = 2^M$	Modulation order
$i = s_k$	Index of start frequency of LFM
$j = s_{k+1}$	Index of end frequency of LFM
$x_{i,j}$	Data LFM modulated i-th and j-th frequencies
E	Power of LFM $x_{i,j}$
N_0	Power of AWGN
x_{TX}	Transmitted LFM from TX
x_{RX}	Demodulated LFM at RX
$\text{P}(*)$	Probability of event $(*)$
e_{s}	The hypothesis of the case in which the demodulation result of the start frequency symbol (i) is an error
e_{e}	The hypothesis of the case in which the demodulation result of the end frequency symbol (j) is an error
c_{s}	The hypothesis of the case in which the demodulation result of the start frequency symbol is correct
c_{e}	The hypothesis of the case in which the demodulation result of the end frequency symbol is correct

Appendix A

In this appendix, it is derived that the BER of the proposed method approximates non-coherent FSK with symbol time length $T_c/2$ in AWGN. The definitions of mathematical symbols are summarized in Abbreviations.

According to the definition in Abbreviations, $P(e_s)$ and $P(e_e)$ are error probabilities of the start frequency and end frequency symbols, respectively. $P(c_s)$ and $P(c_e)$ become correct demodulation probabilities of start frequency and end frequency symbols. Then, $P(c_s)$ becomes $1 - P(e_s)$. If x_{TX} and x_{RX} are $x_{i,j}$ and $x_{\hat{i},\hat{j}}$, $P(c_s)$ can be expressed as

$$P(c_1) = \sum_{i=1}^{K} \sum_{j=1}^{K} \sum_{\hat{j}=1}^{K} P\left(x_{RX} = x_{i,j} | x_{TX} = x_{i,j}\right). \tag{A1}$$

The proposed demodulator calculates the correlation between $x_{i,j}$ and $x_{\hat{i},\hat{j}}$ to decide RX symbols. Let $R_{i,j,\hat{i},\hat{j}}$ be correlator output between $x_{i,j}$ and $x_{\hat{i},\hat{j}}$. It is obtained as

$$R_{i,j,\hat{i},\hat{j}} = \left(x_{i,j}(t) + n(t)\right) \star x_{\hat{i},\hat{j}}(t) \tag{A2}$$

In Equation (A2), $n(t)$ is AWGN. The proposed demodulation is the non-coherent based method, and the correlator output ($R_{i,j,\hat{i},\hat{j}}$) is the Rayleigh distribution [35,36]. $P(c_1)$ is the probability that $R_{i,j,\hat{i},\hat{j}}(i = \hat{i})$ is greater than $R_{i,j,\hat{i},\hat{j}}(i \neq \hat{i})$. It is explained through an example in which both i and j are one ($x_{TX} = x_{1,1}$). The probability that $\hat{j}$ is a specific value from one to K is $1/K$. Then, $P(c_1 | x_{TX} = x_{1,1})$ is expressed as

$$P(c_1 | x_{TX} = x_{1,1}) = \sum_{\hat{j}=1}^{K} P\left(R_{1,1,2,\hat{j}} < R_{1,1,1,\hat{j}}, \cdots, R_{1,1,K,\hat{j}} < R_{1,1,1,\hat{j}} | x_{TX} = x_{1,1}\right)/K. \tag{A3}$$

When $\hat{j}$ is fixed, events $\left(R_{1,1,2,\hat{j}} < R_{1,1,1,\hat{j}}\right)$, $\left(R_{1,1,3,\hat{j}} < R_{1,1,1,\hat{j}}\right)$,...., $\left(R_{1,1,K,\hat{j}} < R_{1,1,1,\hat{j}}\right)$ are independent because the orthogonality between LFMs is only decided by i. Then, we can rewrite Equation (A3) as

$$P(c_1 | x_{TX} = x_{1,1}) = \sum_{\hat{j}=1}^{K} \prod_{\hat{i}=2}^{K} P\left(R_{1,1,\hat{i},\hat{j}} < R_{1,1,1,\hat{j}} | x_{TX} = x_{1,1}\right)/K. \tag{A4}$$

We consider correlator output $R_{i,j,\hat{i},\hat{j}}$ with the time interval of LFM from zero to $T_c/2$ to simplify Equation (A4). Figure A1 depicts the example signals of the proposed method when x_{TX} is $x_{1,1}$.
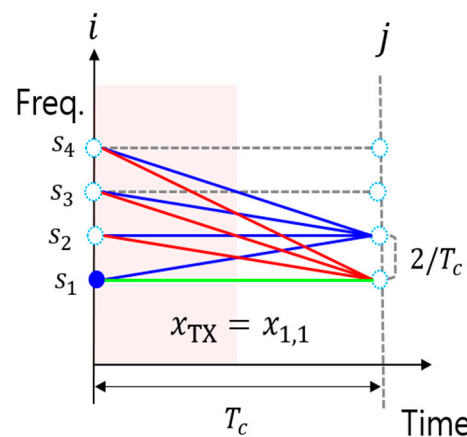

Figure A1. Various examples of the proposed signal.

In Figure A1, the signal from zero to $T_c/2$ significantly affects the correlation between two LFMs (i.e., x_{TX} and x_{RX}) according to $\hat{i}$. Therefore, if we consider the correlator output $R_{i,j,\hat{i},\hat{j}}$ with the time interval from zero to $T_c/2$, we can say that $R_{i,j,\hat{i},\hat{j}}$ is only a random value

of i and $\hat{i}$. Then, the probability that $R_{1,1,1,1}$ is the greatest value among $R_{1,1,1,1} \sim R_{1,1,4,1}$ becomes the same as the probability that $R_{1,1,1,2}$ is the greatest among $R_{1,1,1,2} \sim R_{1,1,4,2}$. $P(x_{TX} = x_{1,1})$ is $1/K^2$. Then, $P(c_1)$ is expressed as

$$P(c_1) \approx \sum_{i=1}^{K} \sum_{j=1}^{K} P\left(R_{1,1,i \neq 1,1} < R_{1,1,1,1}\right)^{K-1}/K^2. \tag{A5}$$

In Equation (A5), as mentioned above, $R_{i,j,\hat{i},\hat{j}}$ is the Rayleigh distribution. Since $R_{i,j,\hat{i},\hat{j}}$ is calculated with only the $T_c/2$ time length, the mean of $R_{1,1,1,1}$ is $E/2$. Therefore, $P(c_1)$ is expressed as

$$P(c_1) \approx \left(\int_0^{R_{1,1,1,1}} \frac{R}{N_0 E/2} e^{-\frac{R^2}{N_0 E/2}} dR \right)^{K-1}. \tag{A6}$$

Using Equation (A6), $P(e_1)$ is obtained as

$$P(e_1) \approx 1 - \left(\int_0^{R_{1,1,1,1}} \frac{R}{N_0 E/2} e^{-\frac{R^2}{N_0 E/2}} dR \right)^{K-1}. \tag{A7}$$

Equation (A7) is the same as the error probability of M-ary non-coherent FSK [35,36] Thus, the BER of the proposed method approximates that of the non-coherent FSK in the AWGN channel. Monte Carlo simulations in AWGN were conducted to verify Equation (A7). The BER of the proposed method and the non-coherent FSK are obtained in the AWGN channel. Then, these results are compared with the theoretical BER curve in Equation (A7). The modulation parameters for the Monte Carlo simulation are represented in Table A1.

Table A1. Modulation parameters for simulation of long-range UWC.

Modulation order (M)	1	2	3	4	5
Bandwidth (B, Hz)	50	150	350	750	1550
Proposed signal length (T_c, ms)			40		
FSK Signal length (T_c, ms)			20		

The simulation results and theoretical BER curve are displayed in Figure A2.
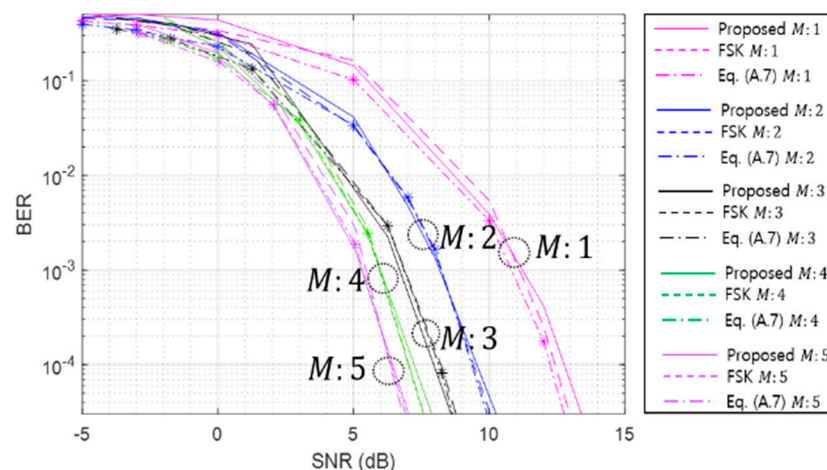

Figure A2. Various examples of the proposed signal.

In Figure A2, the solid line denotes the BER of the proposed method. The BER of FSK obtained through Monte Carlo simulation is shown as the dashed line, and its theoretical BER curve in Equation (A7) is the dotted line. Since the theoretical BER values obtained by Equation (A7) are an approximation, the theoretical values are not exactly the same as the simulation results. However, these results show that the theoretical values from Equation (A7) are almost the same as that of the FSK and those proposed in AWGN.

References

1. Stojanovic, M.; Catipovic, J.; Proakis, J.G. Adaptive multichannel combining and equalization for underwater acoustic communications. *J. Acoust. Soc. Am.* **1993**, *94*, 1621–1631. [CrossRef]
2. Shimura, T.; Watanabe, Y.; Ochi, H.; Song, H.C. Long-range time reversal communication in deep water: Experimental results. *J. Acoust. Soc. Am.* **2012**, *132*, 49–53. [CrossRef] [PubMed]
3. Kang, T.; Song, H.C.; Hodgkiss, W.S. Long-range multi-carrier acoustic communication in deep water using a towed horizontal array. *J. Acoust. Soc. Am.* **2012**, *131*, 4665–4671. [CrossRef]
4. Lee, J.H.; Lee, G.H.; Kim, K.M.; Kim, W.J. Sea trial results of long-range underwater acoustic communication based on frequency modulation in East-Sea. *J. Acoust. Soc. Kor.* **2019**, *38*, 371–377. [CrossRef]
5. Ahn, J.H.; Ra, C.H.; Youn, I.H.; Kim, K.M. Experimental results of underwater acoustic communication with nonlinear frequency modulation wave form. *J. Sensors* **2021**, *21*, 7194. [CrossRef]
6. Huang, J.; Diamant, R. Pre-setting of channel types for long range underwater acoustic communications. In Proceedings of the IEEE Oceans, Marseille, France, 17–20 June 2019. [CrossRef]
7. Huang, J.; Diamant, R. Adaptive Modulation for Long-Range Underwater Acoustic Communication. *IEEE Trans. Wirel. Commun.* **2020**, *19*, 6844–6857. [CrossRef]
8. Song, H.C.; Cho, S.; Kang, T.; Hodgkiss, W.S.; Preston, J.R. Long-range acoustic communication in deep water using a towed array. *J. Acoust. Soc. Am.* **2011**, *129*, 71–75. [CrossRef] [PubMed]
9. Kim, H.; Kim, S.; Choi, J.W.; Bae, H.S. Bidirectional equalization based on error propagation detection in long-range underwater acoustic communication. *Jpn. J. Appl. Phys.* **2019**, *58*, SGGF01. [CrossRef]
10. Pelekanakis, K.; Blouin, S.; Green, D. Performance Analysis of Underwater Acoustic Communications in Barrow Strait. *IEEE J. Ocean. Eng.* **2021**, *46*, 1438–1449. [CrossRef]
11. Kim, D.; Kim, J.; Hahn, J. Long-Range Underwater Communication Based on Time Reversal Processing Using Various Diversity Methods. *Sensors* **2022**, *22*, 3138. [CrossRef]
12. Jinyeong, H.; Junghoon, K.; Yongjin, K. Technology development of unmanned underwater vehicles. *J. Comput. Commun.* **2017**, *5*, 25–35. [CrossRef]
13. Enrica, Z.; Marco, B.; Nikola, M.; Pere, R.; Antonio, P. Challenges and future trends in marine robotics. *J. Annu. Rev. Control* **2018**, *48*, 350–368. [CrossRef]
14. Prasad, M.; Kiran, P.S. Development of Deep Sea Unmanned Underwater Robots: A Survey. In Proceedings of the India Council International, New Delhi, India, 10–13 December 2020. [CrossRef]
15. Nitin, A. Integrating UUVs for naval applications. *J. Marit. Technol. Res.* **2022**, *4*, 3. [CrossRef]
16. Piskur, P.; Szymak, P.; Jaskólski, K.; Flis, L.; Gąsiorowski, M. Hydroacoustic System in a Biomimetic Underwater Vehicle to Avoid Collision with Vessels with Low-Speed Propellers in a Controlled Environment. *Sensors* **2020**, *20*, 968. [CrossRef]
17. Piskur, P.; Szymak, P. Algorithms for passive detection of moving vessels in marine environment. *J. Mar. Eng. Technol.* **2017**, *16*, 377–385. [CrossRef]
18. Plaisant, A. Long range acoustic communications. In Proceedings of the IEEE Oceans'98, Nice, France, 28 September–1 October 1998. [CrossRef]
19. Shimura, T.; Ochi, H.; Watanabe, Y.; Hattori, T. Results of Basic At-Sea Experiments on Time-Reversal Communication in the Deep Ocean. In Proceedings of the IEEE Oceans'08, Kobe, Japan, 9–11 April 2008. [CrossRef]
20. Shimura, T.; Ochi, H.; Watanabe, Y.; Hattori, T. Experiment Results of Time-Reversal Communication at the Range of 300 km. *Jpn. J. Appl. Phys.* **2011**, *49*, 07HG11. [CrossRef]
21. Shimura, T.; Ochi, H.; Song, H.C. Experimental demonstration of multiuser communication in deep water using time reversal. *J. Acoust. Soc. Am.* **2013**, *134*, 3223–3229. [CrossRef]
22. Shimura, T.; Ochi, H.; Watanabe, Y. Time reversal communication in deep ocean results of recent experiments. In Proceedings of the IEEE Symposium on and '11 Workshop on Scientific Use of Submarine Cables and Related Technologies, Tokyo, Japan, 5–8 April 2011. [CrossRef]
23. Zhao, A.; Zeng, C.; Hui, J.; Wang, K.; Tang, K. Study on Time Reversal Maximum Ratio Combining in Underwater Acoustic Communications. *Appl. Sci.* **2021**, *11*, 1509. [CrossRef]
24. Youn, C.H.; Ra, H.I.; An, J.H.; Kim, K.M.; Kim, I.S. Experimental analysis of very long range spread spectrum underwater acoustic communication using vertical sensor array. *J. Acoust. Soc. Kor.* **2021**, *41*, 150–158. [CrossRef]
25. Urick, R.J. *Principles of Underwater Sound*, 3rd ed.; MacGraw-Hill: New York, NY, USA, 1983.
26. John, L.; Maurice, E.; Chaim, L.P. *Propagation of Sound in the Ocean*; Geological Society of America: New York, NY, USA, 1948.
27. Higley, W.J.; Roux, P.; Kuperman, W.A.; Hodgkiss, W.S.; Song, H.C.; Akal, T.; Stevenson, M. Synthetic aperture time-reversal communications in shallow water: Experimental demonstration at sea. *J. Acoust. Soc. Am.* **2005**, *118*, 2365–2372. [CrossRef]
28. Song, H.C.; Hodgkiss, W.S.; Kuperman, W.A.; Akal, T.; Stevenson, M. High-rate synthetic aperture communications in shallow water. *J. Acoust. Soc. Am.* **2009**, *126*, 3057–3061. [CrossRef] [PubMed]
29. Song, H.C.; Dzieciuch, M. Feasibility of global-scale synthetic aperture communications. *J. Acoust. Soc. Am.* **2009**, *125*, 8–10. [CrossRef] [PubMed]
30. Su, Y.; Liu, X.; Jin, Z.; Fu, X. Fast Estimation of Underwater Acoustic Multipath Channel Based on LFM Signal. In Proceedings of the Global Oceans, Biloxi, MS, USA, 5–30 October 2020. [CrossRef]

31. Ahn, J.; Do, D.; Kim, W. The Long-Range Biomimetic Covert Communication Method Mimicking Large Whale. *Sensors* **2022**, *22*, 8011. [CrossRef] [PubMed]
32. Chung, W.; Johnson, C.; Ready, M. Characterization of multipath distortion of FSK signals. *IEEE Signal Process. Lett.* **2002**, *9*, 26–28. [CrossRef]
33. Fan, W.W.; Liu, L.; Zhang, Y.W.; Dong, J.G.; Sun, D.J. An MMSE Approach to Channel Shorting for Underwater Acoustic FH-FSK Communication. *Appl. Mech. Mater.* **2014**, *511–512*, 334–341. [CrossRef]
34. Ren, H.; Hu, X.; Xu, F.; Jun, X.; Qing, W.; Zhan, C.; Chen, Y. SNR estimation algorithm of LFM signal based on FRFT for long range and shallow underwater acoustic communication systems. In Proceedings of the Oceans 2014, Taipei, Taiwan, 7–10 April 2014. [CrossRef]
35. Proakis, J.G. *Digital Communication*, 4th ed.; McGraw-Hill: Boston, MA, USA, 2000; pp. 310–311.
36. Xiong, F. *Digital Modulation Techniques*, 1st ed.; Artech House: Boston, MA, USA; London, UK, 2000; pp. 621–625.